# Finite element modelling of sandwich panels with graded core under various boundary conditions

**M. Kashtalyan**
**m.kashtalyan@abdn.ac.uk**

**B. Woodward**

Centre for Micro- and Nanomechanics (CEMINACS), School of Engineering
University of Aberdeen
Aberdeen, UK

## ABSTRACT

Sandwich panels are widely used in the aerospace industry instead of solid plates due to their high flexural stiffness-to-weight and flexural strength-to-weight ratios. However due to the mismatch of properties between the face sheets and the core, stress concentrations can occur at the face sheet/core interfaces, often leading to delamination. One possible solution to this problem is the introduction of a graded core — a core in which the properties vary gradually from the face sheets to the core centre, eliminating any abrupt changes in properties. In this paper a 3D finite element method, fully validated through comparison with results from the literature and a 3D elasticity solution, is applied to modelling of sandwich panels with graded core. The approach makes use of graded elements to study the effect of varying the boundary conditions on the elastic deformation of the panel subject to uniformly distributed loading. Comparative analysis of stress and displacement fields in sandwich panels with homogeneous and graded cores is carried out under various combinations of simply supported, clamped and free edges.

## NOMENCLATURE

| | |
|---|---|
| $a$,$b$ | panel dimensions |
| $D$ | flexural rigidity |
| $E$ | Young's modulus |
| $G_f$, $G_c$ | shear moduli of the face sheets and the core |
| $G^{(k)}$ | shear modulus of layer $k$ |

**Paper No. 3866**. Manuscript received 22 June 2012, revised version received 22 September 2012, accepted 19 October 2012.

| | |
|---|---|
| $2h_c$, $h_f$ | core thickness, face sheet thickness |
| $h_0 = 2h$ | panel thickness |
| $k$ | layer number |
| $M_{11}^{(k)}$, $M_{22}^{(k)}$ | bending moments per unit length of layer $k$ |
| $q_0$ | uniformly distributed load |
| $u_i^{(k)}$ | components of displacement vector of layer $k$ |
| $V_1^{(k)}$, $V_2^{(k)}$ | out-of-plane shear forces per unit length of layer $k$ |
| $x_1$, $x_2$, $x_3$ | Cartesian co-ordinates |
| $\gamma^{(k)}$ | inhomogeneity parameter of layer $k$ |
| $\nu^{(k)}$ | Poisson's ratio of layer $k$ |
| $\sigma_{ij}^{(k)}$ | components of stress tensor of layer $k$ |

# 1.0 INTRODUCTION

Sandwich panels, consisting of a core covered by face sheets, are widely used in the aerospace industry instead of solid plates due to their high flexural stiffness-to-weight and flexural strength-to weight ratios. Due to the mismatch in stiffness properties between the face sheets and the core, sandwich panels are susceptible to delamination, caused by high interfacial stresses, especially under localised or impact loading[1,2].

One effective method of minimising the large interfacial shear stresses is to make use of a graded material for the panel core. Functionally graded materials are a type of heterogeneous composite materials exhibiting gradual variation in microstructure and composition of the two constituent materials from one surface of the material to the other, resulting in properties which vary continuously across the material.

A number of researchers have presented analytical solutions for sandwich panels with graded core: Anderson[3] developed a three dimensional (3D) elasticity solution for a sandwich panel with orthotropic face sheets and an isotropic functionally graded core subjected to transverse loading by a rigid sphere. Kashtalyan and Menshykova[4] and Woodward and Kashtalyan[5-6] recently developed 3D elasticity solutions for sandwich panels with functionally graded core whose shear moduli vary exponentially through the thickness of the core. Apetre *et al*[7] investigated several available sandwich beam theories for their suitability of application to sandwich plates with functionally graded core. All of the above studies assume that the panel is simply supported on all of the edges. However in reality there are many other combinations of boundary conditions which may be encountered.

Bian *et al*[8] examined the one-dimensional (1D) problem of a functionally graded plate under cylindrical bending through use of a modified classical plate theory. An analysis of stresses and displacements for plates with the following boundary conditions were considered: two opposite edges simply supported; one edge clamped and the other simply supported; two opposite edges clamped and one edge clamped and the other edge free were considered. A two-dimensional analysis (2D) of a functionally graded cantilever beam with exponential variation in stiffness properties was carried out by Zhong *et al*[9]. Using Airy stress functions, stresses and displacements were compared under a number of different loads including a concentrated shear force at the free edge and uniform pressure on the top surface. Xu and Zhou[10] considered a functionally graded plate with exponential variation in stiffness properties and with variable thickness. Using displacement functions, two plates, one with convex lower surface, the other with concave lower surface but both simply supported, are analysed on the basis of 3D elasticity theory.

https://doi.org/10.1017/S0001924000007648 Published online by Cambridge University Press

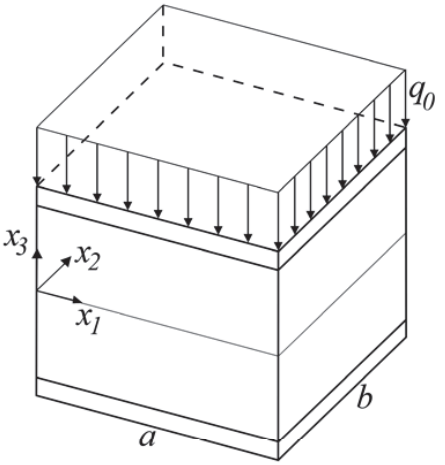


Figure 1. Sandwich panel under uniformly distributed loading.

Once more employing displacement functions, Xu *et al*[11] carried out a 2D stress analysis of a variable thickness beam with one end clamped and the other simply supported. They found that their solution could be applied to the analysis of stress and displacement distributions of arbitrarily and continuously varying thickness beams.

A functionally graded plate with exponential variation in Young's modulus resting on a Winkler Pasternak elastic foundation was studied by Huang and Chen[12]. The state space method was used to develop a 3D elasticity solution to the problem which was then used to study the effects of stiffness of the foundation, loading cases and gradient index on the mechanical behaviour of the plate. Sburlati and Bardella[13] considered a functionally graded circular plate with clamped edges. Displacement functions were used to formulate a 3D solution of the stresses and displacement through the plate thickness and it is shown that under certain combinations of boundary conditions and loading a non-planar neutral surface exists.

In the current work, the effect of various boundary conditions on the elastic deformation of a sandwich panel containing a functionally graded core and subjected to uniformly distributed loading is considered. The analysis utilises a 3D finite element simulation, fully validated by comparison with a 3D analytical elasticity solution, using ABAQUS software and user implemented graded elements. Stresses and displacements are calculated through the thickness of the panel under combinations of simply supported, clamped and free boundary conditions and are then compared with those in a reference panel containing a homogenous core.

## 2.0 PROBLEM FORMULATION

Let us consider a sandwich panel (Fig. 1) of length $a$, width $b$ and total thickness $h_0 = 2h$ is referred to a Cartesian co-ordinate system $x_1, x_2, x_3$ ($0 \le x_1 \le a$, $0 \le x_2 \le b$, $-h \le x_3 \le b$), so that the panel is symmetric with respect to the mid-plane $x_3 = 0$ . Let us assume the panel consists of four layers ($k = 1, ..., 4$), with layers 1 & 4 being the face sheets of thickness $h_f$, and layers 2 & 3 being the core of thickness $2h_c$, which is subdivided into two layers for the sake of convenience. The face sheets are assumed to be homogeneous with the shear modulus $G^{(1)} = G^{(4)}$

https://doi.org/10.1017/S0001924000007648 Published online by Cambridge University Press

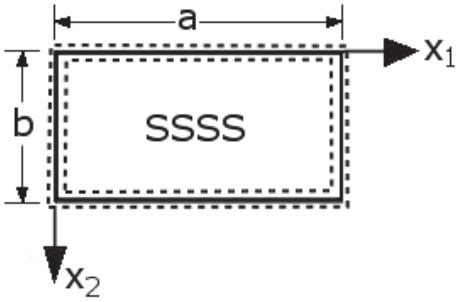


Figure 2. Geometry and co-ordinates of panel with all edges simply supported.

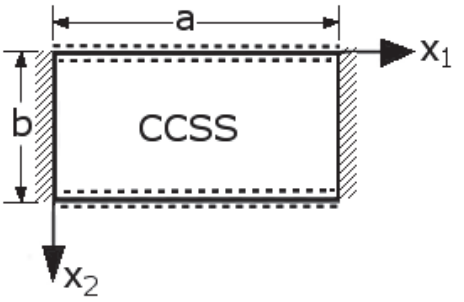


Figure 3. Geometry and co-ordinates of panel with two edges clamped and two simply supported.

$= G_f = const$ , while the shear moduli of the core are assumed to vary exponentially through the thickness from the $G_f$ value at the face sheet/core interface to the $G_f$ value at the mid-plane according to

$$G^{(k)}(x_3) = G_c \exp\left(\gamma^{(k)} \frac{x_3}{h}\right), \quad k = 2,3 \qquad \ldots (1)$$

where $\gamma^{(k)}$ are the inhomogeneity parameters

$$\gamma^{(k)} = (-1)^k \frac{h}{h_c} \ln \frac{G_c}{G_f}, \quad k = 2,3 \qquad \ldots (2)$$

Both face sheets and core are assumed to have constant Poisson's ratios $\nu^{(k)} = const$ ($k = 1, \ldots 4$).

The face sheets are assumed to be perfectly bonded to the core, so that the continuity of stresses and displacements exists at the face sheet/core interfaces, i.e.

$$x_3 = x_3^{(1)}: \quad \sigma_{i3}^{(2)} - \sigma_{i3}^{(1)} = 0, \quad u_i^{(2)} - u_i^{(1)} = 0, \quad i = x_1, x_2, x_3 \qquad \ldots (3a)$$

$$x_3 = x_3^{(3)}: \quad \sigma_{i3}^{(4)} - \sigma_{i3}^{(3)} = 0, \quad u_i^{(4)} - u_i^{(3)} = 0, \quad i = x_1, x_2, x_3 \qquad \ldots (3b)$$

where $\sigma_{ij}^{(k)}$ and $u_i^{(k)}$ ($k = 1, \ldots,4$) are the components of the stress tensor and displacement vector, respectively. The panel is subjected to uniformly distributed loading of magnitude $q_0$ on the top surface, while the so lower surface remains load free (Fig. 1).

The behaviour of the panel under a number of different boundary conditions will be investigated. A four-letter notation is used to describe the each set of boundary: the first letter describes the boundary conditions on the edge $x_1 = 0$, the second on the edge $x_1 = a$, third on the edge $x_2 = 0$, and the fourth on the edge $x_2 = b$. The letter *S* stands for a simply supported edge, where both edge displacement and edge bending moment are equal to zero; the letter *C* stands for a clamped edge, where the edge displacement and edge slope are zero; the letter *F* stands for a free edge, where both edge bending moment and edge shear force are zero.

The following cases are considered in this study:

**(*i*) Panel with all edges simply supported (SSSS)**

First, we consider a panel (Fig. 2) with all edges simply supported, so that

$$x_1 = 0, a: \quad u_3^{(k)} = 0, \quad M_{11}^{(k)} = 0 \quad k = 1, \ldots, 4 \qquad \ldots (4a)$$

https://doi.org/10.1017/S0001924000007648 Published online by Cambridge University Press

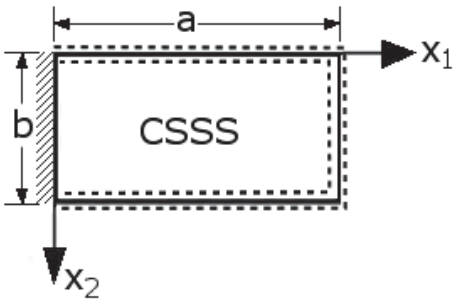


Figure 4. Geometry and co-ordinates of panel with one edge clamped and three edges simply supported.

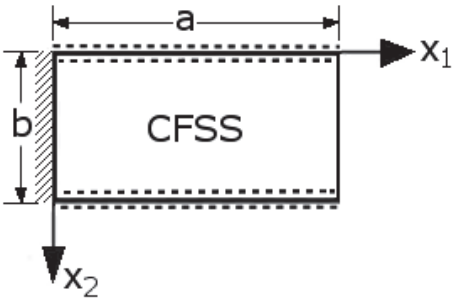


Figure 5. Geometry and co-ordinates of panel with one edge clamped opposite edge free and other edges simply supported.

$$x_2 = 0, b: \quad u_3^{(k)} = 0, \quad M_{22}^{(k)} = 0 \quad k = 1,\ldots,4 \qquad \ldots (4b)$$

**(*ii*) Panel with two opposite edges clamped and two simply supported (CCSS)**

The second panel under consideration (Fig. 3) has the edges at $x_1 = 0, a$ clamped and those at $x_2 = 0, b$ simply supported. The boundary conditions are thus:

$$x_1 = 0, a: \quad u_3^{(k)} = 0, \quad \frac{\partial u_3^{(k)}}{\partial x_1} = 0 \quad k = 1,\ldots,4 \qquad \ldots (5a)$$

$$x_2 = 0, b: \quad u_3^{(k)} = 0, \quad M_{22}^{(k)} = 0 \quad k = 1,\ldots,4 \qquad \ldots (5b)$$

**(*iii*) Panel with one edge clamped and all other edges simply supported (CSSS)**

Consider the panel (Fig. 4) which has the edge at $x_1 = 0$ clamped and those at $x_1 = a$ and $x_2 = 0, b$ simply supported. The boundary conditions are thus:

$$x_1 = 0: \quad u_3^{(k)} = 0, \quad \frac{\partial u_3^{(k)}}{\partial x_1} = 0 \quad k = 1,\ldots,4 \qquad \ldots (6a)$$

$$x_1 = a: \quad u_3^{(k)} = 0, \quad M_{11}^{(k)} = 0 \quad k = 1,\ldots,4 \qquad \ldots (6b)$$

$$x_2 = 0, b: \quad u_3^{(k)} = 0, \quad M_{22}^{(k)} = 0 \quad k = 1,\ldots,4 \qquad \ldots (6c)$$

**(*iv*) Panel with one edge clamped, opposite edge free and other edges simply supported (CFSS)**

Consider the panel (Fig. 5) which has the edge at $x_1 = 0$ clamped, the edge at $x_1 = a$ free and the edges at $x_2 = 0, b$ simply supported. The boundary conditions are thus:

$$x_1 = 0: \quad u_3^{(k)} = 0, \quad \frac{\partial u_3^{(k)}}{\partial x_1} = 0 \quad k = 1,\ldots,4 \qquad \ldots (7a)$$

$$x_1 = a: \quad M_{11}^{(k)} = 0, \quad V_1^{(k)} = 0 \quad k = 1,\ldots,4 \qquad \ldots (7b)$$

$$x_2 = 0, b: \quad u_3^{(k)} = 0, \quad M_{22}^{(k)} = 0 \quad k = 1,\ldots,4 \qquad \ldots (7c)$$

https://doi.org/10.1017/S0001924000007648 Published online by Cambridge University Press

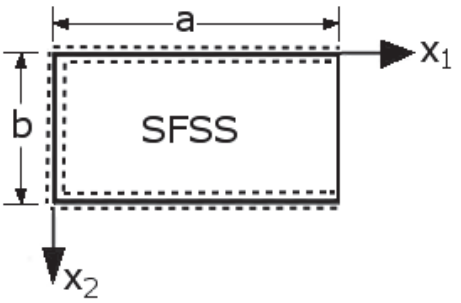


Figure 6. Geometry and co-ordinates of panel with one edge free and other edges simply supported.

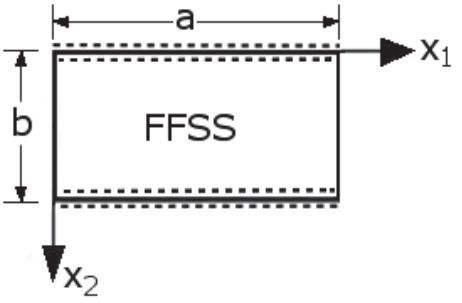


Figure 7. Geometry and co-ordinates of panel with two opposite edges free and two simply supported.

**(*v*) Panel with three simply supported edges and one free edge (SFSS)**

Consider the panel (Fig. 6) which has the edges at $x_1 = 0$ and $x_2 = 0b$ simply supported and the edge at $x_1 = a$ free. The boundary conditions are thus:

$$x_1 = 0: \quad u_3^{(k)} = 0, \quad M_{11}^{(k)} = 0 \quad k = 1,\ldots,4 \qquad \ldots (8a)$$

$$x_1 = a: \quad M_{11}^{(k)} = 0, \quad V_1^{(k)} = 0 \quad k = 1,\ldots,4 \qquad \ldots (8b)$$

$$x_2 = 0,b: \quad u_3^{(k)} = 0, \quad M_{22}^{(k)} = 0 \quad k = 1,\ldots,4 \qquad \ldots (8c)$$

**(*vi*) Panel with two opposite edges free and two simply supported (FFSS)**

Consider the panel (Fig. 7) which has the edges at $x_1 = 0$ free and those at $x_2 = 0b$ simply supported. The boundary conditions are thus:

$$x_1 = 0,a: \quad M_{11}^{(k)} = 0, \quad V_1^{(k)} = 0 \quad k = 1,\ldots,4 \qquad \ldots (9a)$$

$$x_2 = 0,b: \quad u_3^{(k)} = 0, \quad M_{22}^{(k)} = 0 \quad k = 1,\ldots,4 \qquad \ldots (9b)$$

**(*vii*) Panel with one edge clamped and all other edges free (CFFF)**

Consider the panel (Fig. 8) which has the edge at $x_1 = 0$ clamped and those at $x_1 = a$ and $x_2 = 0b$ free. The boundary conditions are thus:

$$x_1 = 0: \quad u_3^{(k)} = 0, \quad \frac{\partial u_3^{(k)}}{\partial x_1} = 0 \quad k = 1,\ldots,4 \qquad \ldots (10a)$$

$$x_1 = a: \quad M_{11}^{(k)} = 0, \quad V_1^{(k)} = 0 \quad k = 1,\ldots,4 \qquad \ldots (10b)$$

$$x_2 = 0,b: \quad M_{22}^{(k)} = 0, \quad V_2^{(k)} = 0 \quad k = 1,\ldots,4 \qquad \ldots (10c)$$

**(*viii*) Panel with one edge clamped, two free edges and one edge simply supported (CFSF)**

Consider the panel (Fig. 9) which has the edge at $x_1 = 0$ clamped, the edge at $x_2 = 0$ simply supported and those at $x_1 = a$ and $x_2 = b$ free. The boundary conditions are thus:

https://doi.org/10.1017/S0001924000007648 Published online by Cambridge University Press

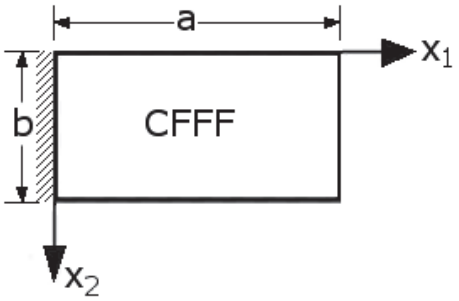


Figure 8. Geometry and co-ordinates of panel with one edge clamped and all other edges free.

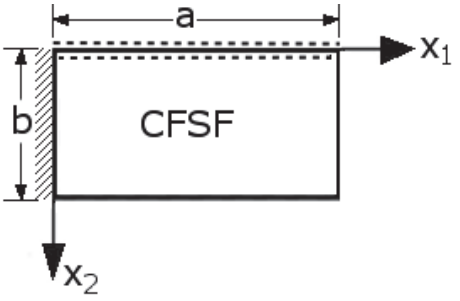


Figure 9. Geometry and co-ordinates of panel with one edge clamped, two free edges and one edge simply supported.

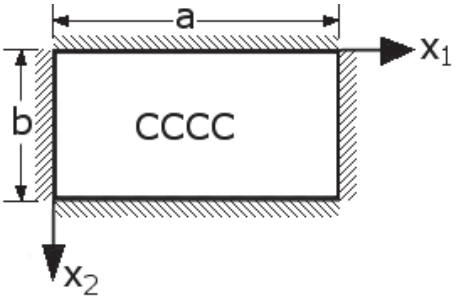


Figure 10. Geometry and co-ordinates of panel with all edges clamped.

$$x_1 = 0: \quad u_3^{(k)} = 0, \quad \frac{\partial u_3^{(k)}}{\partial x_1} = 0 \quad k = 1,\ldots,4 \qquad \ldots (11a)$$

$$x_1 = a: \quad M_{11}^{(k)} = 0, \quad V_1^{(k)} = 0 \quad k = 1,\ldots,4 \qquad \ldots (11b)$$

$$x_2 = 0: \quad u_3^{(k)} = 0, \quad M_{22}^{(k)} = 0 \quad k = 1,\ldots,4 \qquad \ldots (11c)$$

$$x_2 = b: \quad M_{22}^{(k)} = 0, \quad V_2^{(k)} = 0 \quad k = 1,\ldots,4 \qquad \ldots (11d)$$

**(*ix*) Panel with all edges clamped (CCCC)**

Consider the panel (Fig. 10) which has all edges clamped. The boundary conditions are thus:

$$x_1 = 0, a: \quad u_3^{(k)} = 0, \quad \frac{\partial u_3^{(k)}}{\partial x_1} = 0 \quad k = 1,\ldots,4 \qquad \ldots (12a)$$

$$x_2 = 0, b: \quad u_3^{(k)} = 0, \quad \frac{\partial u_3^{(k)}}{\partial x_2} = 0 \quad k = 1,\ldots,4 \qquad \ldots (12b)$$

## 3.0 FINITE ELEMENT MODELLING

In order to accurately model the functionally graded core material, the 3D finite element method used in the present study employs elements with stiffness gradient in the thickness

https://doi.org/10.1017/S0001924000007648 Published online by Cambridge University Press

direction. The method of element formulation is discussed in detail in a number of papers[14-17] and an overview is given here. Beginning with an assumed set of shape functions it can be written that the displacements within an element are interpolated as

$$u(x) = \sum_{i=1}^{n} N_i(x) U_i \quad \ldots (13a)$$

where $\mathbf{N_i(x)}$ is a matrix of shape functions corresponding to each of the $n$ nodes of the element and $U_i$ are nodal displacements corresponding to each of the $n$ nodes.

To obtain the element strains differentiation of the displacements is carried out, hence

$$\varepsilon(x) = \sum_{i=1}^{n} B_i(x) U_i \quad \ldots (13b)$$

where $\mathbf{B_i(x)}$ is a matrix of derivatives of the shape functions. For linear elastic behaviour standard stress strain relations can now be used

$$\sigma(x) = C(x)\varepsilon(x) \quad \ldots (14)$$

where $\mathbf{C(x)}$ is the material property matrix. Traditionally this matrix contains constant material properties but for a functionally graded material can be set to spatially variable functions, for example exponential variation in Young's modulus.

The element stiffness matrix $\mathbf{k^e}$, mapping the nodal displacements $U_i$, to the nodal forces $f_i$, can be written in the same way as for a standard finite element, that is:

$$f_i = k^e U_i \quad \ldots (15)$$

Now applying the theorem of virtual work which states that the work done by nodal forces must be equal to the work of deformation within the element, allows the following to be written:

$$k^e = \int_{V_e} B^T(x) C(x) B(x) \mathrm{d}V \quad \ldots (16)$$

where $V_e$ is the volume of the element. Analytical integration of this expression is very difficult or indeed impossible, so instead a numerical integration scheme is applied. Through application of Gauss quadrature (see Ref. 8), Equation (16) can be calculated in the following manner

$$k^e = \sum_{i=1}^{n}\sum_{j=1}^{n}\sum_{k=1}^{n} W_i W_j W_k B_{ijk}^T(x) C_{ijk}(x) B_{ijk}(x) J_{ijk} \quad \ldots (17)$$

where $W_i$, $W_j$, $W_k$ are Gauss weights (specified in Ref. 19), $i$, $j$ and $k$ are the Gaussian integration points and $J_{ijk}$ is the determinant of the Jacobian matrix. In carrying out this integration, the constitutive matrix is evaluated at each Gaussian integration point and since the applied loading is known then displacements can be found through application of:

$$U_i = k^{e-1} f \quad \ldots (18)$$

Commercial finite element software such as ABAQUS does not support graded elements directly, therefore they have to be defined separately in a user subroutine. In ABAQUS this is

https://doi.org/10.1017/S0001924000007648 Published online by Cambridge University Press

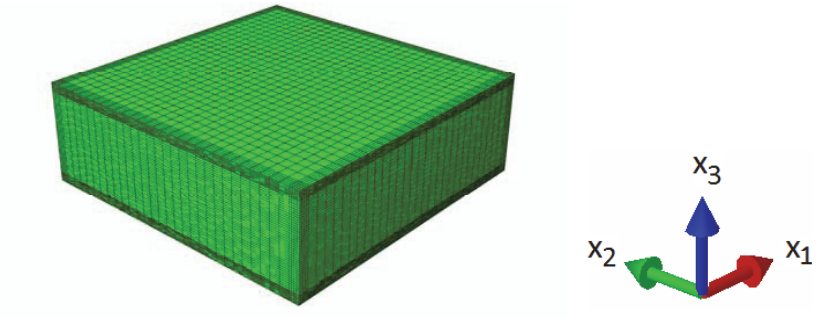


Figure 11. Undeformed sandwich panel with mesh.

carried out through a UMAT subroutine (see Ref. 20). This subroutine is called at all material calculation points of elements for which the material definition includes a user-defined material and is used to define the mechanical constitutive behaviour of the material and provide the material Jacobian matrix, $\frac{\partial \Delta\sigma}{\partial \Delta\varepsilon}$. Most importantly the stresses and solution-dependent state variables are calculated and updated to their values at the end of the increment for which the subroutine is called. In order to accurately model the problem, the mesh shown in Fig. 11 is used, utilising 20 node quadrilateral elements. The face sheets comprise $36 \times 36 \times 5$ homogeneous elements, whilst each half of the core is modelled by $36 \times 36 \times 25$ elements whose stiffness is graded in the $x_3$ direction when modelling the panel with FGM core and by $36 \times 36 \times 25$ homogenous elements when modelling the panel with HC core. The mesh is refined such that there are more elements around the face sheet/core interface to ensure that the abrupt property change for the panel with HC core is captured in detail.

## 4.0 VALIDATION

The developed finite element model for graded materials is validated through comparison with the available 3D solutions for isotropic functionally graded plates[21]. Table 1 shows normalised mid-plane displacements $\bar{u}_3 = \frac{G_1 u_3}{q_0 h}$ at the centre of a square ($a = b$) isotropic graded plate with exponential variation of the shear modulus through the thickness based on the present finite element solution and the 3D elasticity solution[22]. The plate is simply supported on its edges and loaded by transverse loading $Q(x_1, x_2) = -q_0 \ \mathrm{Sin}(\pi x_1/a)\mathrm{Sin}(\pi x_2/b)$ at the top surface. The results are given for a range of inhomogeneity parameters $\gamma$. The finite element solution is found to be in excellent agreement with the 3D elasticity solution, the difference in transverse displacements being at its largest 0·009%.

As the finite element analysis is going to be used exclusively in the present analysis of the sandwich panels under different boundary conditions, it is important that the modelling of these different conditions is validated too. A finite element model (containing $20 \times 20 \times 10$ elements for square plates and $20 \times 30 \times 10$ elements for rectangular plates) is created and is used to analyse a homogenous isotropic plate under uniformly distributed loading for which results already exist

https://doi.org/10.1017/S0001924000007648 Published online by Cambridge University Press

**Table 1**

**Displacement $\bar{u}_3 = \frac{G_1 u_3}{q_0 h}$ at the centre (*a*/2, *b*/2, *h*/2) of a thick square simply supported plate calculated using 3D elasticity solution and FE analysis**

| γ | 3D elasticity solution[22] | Present FE model | Difference (%) |
|---|---|---|---|
| 0·1 | –1·28002 | –1·2799 | 0·009014 |
| 0·01 | –1·33617 | –1·33606 | 0·008545 |
| 0·001 | –1·34192 | –1·3418 | 0·008596 |
| 0·0001 | –1·34249 | –1·34238 | 0·008249 |
| 0·00001 | –1·34255 | –1·34244 | 0·008066 |
| 0·000001 | –1·34255 | –1·34244 | 0·008495 |
| –0·000001 | –1·34256 | –1·34244 | 0·00859 |
| –0·00001 | –1·34256 | –1·34245 | 0·008274 |
| –0·0001 | –1·34262 | –1·34251 | 0·008092 |
| –0·001 | –1·34319 | –1·34308 | 0·00851 |
| –0·01 | –1·34896 | –1·34885 | 0·008434 |
| –0·1 | –1·40795 | –1·40784 | 0·007871 |

**Table 2**

**Normalised displacement $\bar{u}_3 = \frac{D u_3(a/2, b/2, h)}{q_0 b^4} \times 10^2$ for isotropic rectangular plate with two edges clamped and two simply supported**

| CCSS | *b*/*a* = 1/3 | *b*/*a* = 1/2 | *b*/*a* = 1 | *b*/*a* = 3/2 | *b*/*a* = 2 | *b*/*a* = 3 |
|---|---|---|---|---|---|---|
| Reddy[23] | 1·1681 | 0·8445 | 0·1917 | 0·2476 | 0·2612 | 0·2619 |
| Present FE model | 1·166967 | 0·842381 | 0·1908 | 0·245473 | 0·259271 | 0·2596 |
| Difference (%) | –0·09712 | –0·25155 | –0·4717 | –0·8664 | –0·74384 | –0·88598 |

**Table 3**

**Normalised displacement $\bar{u}_3 = \frac{D u_3(a/2, b/2, h)}{q_0 b^4} \times 10^2$ for isotropic rectangular plate with one edge clamped and three edges simply supported**

| CSSS | *b*/*a* = 1/2 | *b*/*a* = 1 | *b*/*a* = 3/2 | *b*/*a* = 2 | *b*/*a* = 3 |
|---|---|---|---|---|---|
| Reddy[23] | 0·927 | 0·2786 | 0·425 | 0·488 | 0·5193 |
| Present FE model | 0·92595 | 0·2779 | 0·423079 | 0·486081 | 0·5167 |
| Difference (%) | –0·1134 | –0·25189 | –0·45408 | –0·3948 | –0·50319 |

in the literature[23]. Tables 2-6 show non-dimensional displacements $\bar{u}_3 = \frac{D u_3(a/2, b/2, h)}{q_0 b^4} \times 10^2$ where $D = \frac{E h^3}{12(1-\nu^2)}$ is the flexural rigidity of the plate, calculated using the current finite

https://doi.org/10.1017/S0001924000007648 Published online by Cambridge University Press

**Table 4**

**Normalised displacement $\bar{u}_3 = \dfrac{Du_3(a,b/2,h)}{q_0 b^4}$ for isotropic rectangular plate with one edge clamped opposite edge free and other edges simply supported**

| CFSS | $b/a = 1$ | $b/a = 3/2$ | $b/a = 2$ | $b/a = 3$ |
|---|---|---|---|---|
| Reddy[23] | 0·0112 | 0·0335 | 0·0582 | 0·094 |
| Present FE model | 0·0112 | 0·033499 | 0·058207 | 0·0938 |
| Difference (%) | 0 | –0·004 | 0·012271 | –0·21322 |

**Table 5**

**Normalised displacement $\bar{u}_3 = \dfrac{Du_3(a,b/2,h)}{q_0 b^4}$ for isotropic rectangular plate with one edge free and other edges simply supported**

| SFSS | $b/a = 1/3$ | $b/a = 1/2$ | $b/a = 1$ | $b/a = 3/2$ | $b/a = 2$ | $b/a = 3$ |
|---|---|---|---|---|---|---|
| Reddy[23] | 0·01521 | 0·01507 | 0·01285 | 0·00968 | 0·00709 | 0·00399 |
| Present FE model | 0·015212 | 0·015075 | 0·0129 | 9·68E–03 | 0·007105 | 0·003995 |
| Difference (%) | 0·010017 | 0·031431 | 0·387597 | –0·00413 | 0·20443 | 0·115676 |

**Table 6**

**Normalised displacement $\bar{u}_3 = \dfrac{Du_3(a/2,b/2,h)}{q_0 b^4}$, for isotropic rectangular plate with two edges free and other edges simply supported**

| FFSS | $b/a = 1$ |
|---|---|
| Reddy[23] | 0·01309 |
| Present FE model | 0·0131 |
| Difference (%) | 0·076336 |

element method for various aspect ratios of thin plates under different boundary conditions. Results are found to be in good agreement with those of Reddy[21].

## 5.0 RESULTS AND DISCUSSION

In this section, comparative study of uniformly loaded sandwich panels is presented for nine different combinations of boundary conditions: SSSS, CCSS, CSSS, CFSS, SFSS, FFSS, CFFF, CFSF and CCCC. The stress and displacements fields in a panel with functionally graded core (FGMC panel) and homogeneous core (HC panel) are compared. Both panels are thick, with $a/h_0 = b/h_0 = 3$, and the thickness of the face sheets is $h_f = 0{\cdot}05h_0$. The shear moduli ratio for both panels is $G_f/G_c = 10$, and the Poisson's ratios are taken as $\nu^{(k)} = 0{\cdot}3$, $k = 1, ..., 4$. The inhomogeneity parameters for the graded core of the FGMC panel are determined from Equation (2).

Figures 12-29 show the variation of normalised stresses $\bar{\sigma}_{ij} = \sigma_{ij}/q_0$ and normalised

https://doi.org/10.1017/S0001924000007648 Published online by Cambridge University Press

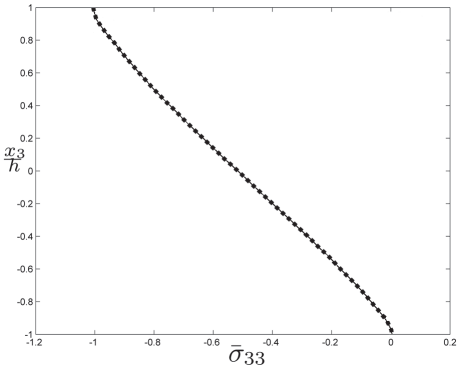


Figure 12. Through-thickness variation of the normalised out-of-plane normal stress $\sigma_{33}(0{\cdot}5a, 0{\cdot}5b, x_3)$ for all studied boundary conditions, HC panel and FGMC panel.

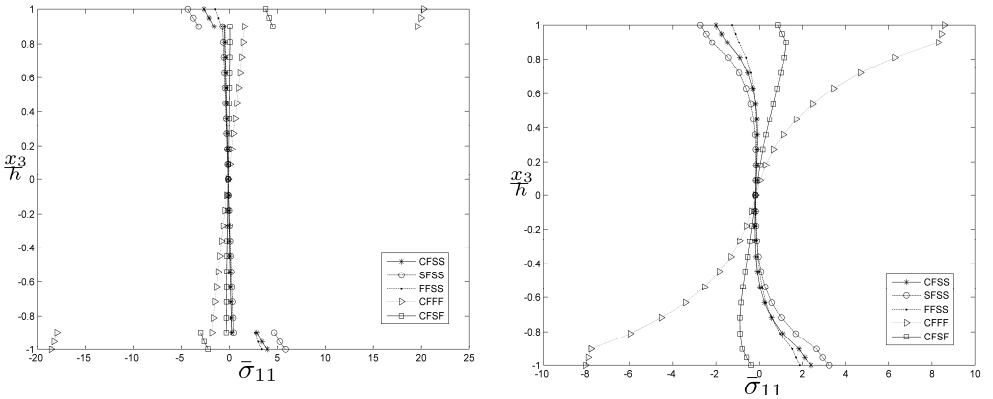


Figure 13. Through-thickness variation of the normalised in-plane normal stress $\bar{\sigma}_{11}(0{\cdot}5a, 0{\cdot}5b, x_3)$ for a range of boundary conditions (CFSS, SFSS, FFSS, CFFF & CFSF) in (a) HC panel, (b) FGMC panel.

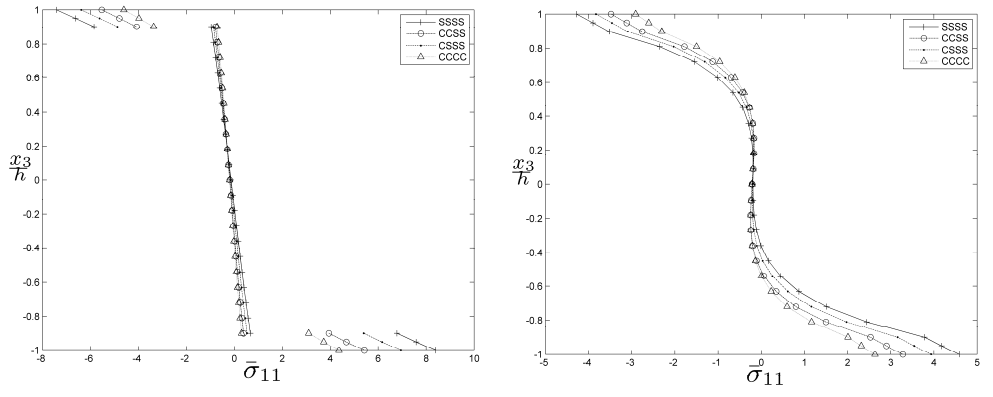


Figure 14. Through-thickness variation of the normalised in-plane normal stress $\bar{\sigma}_{11}(0{\cdot}5a, 0{\cdot}5b, x_3)$ for a range of boundary conditions (SSSS, CCSS, CSSS & CCCC) in (a) HC panel, (b) FGMC panel.

https://doi.org/10.1017/S0001924000007648 Published online by Cambridge University Press

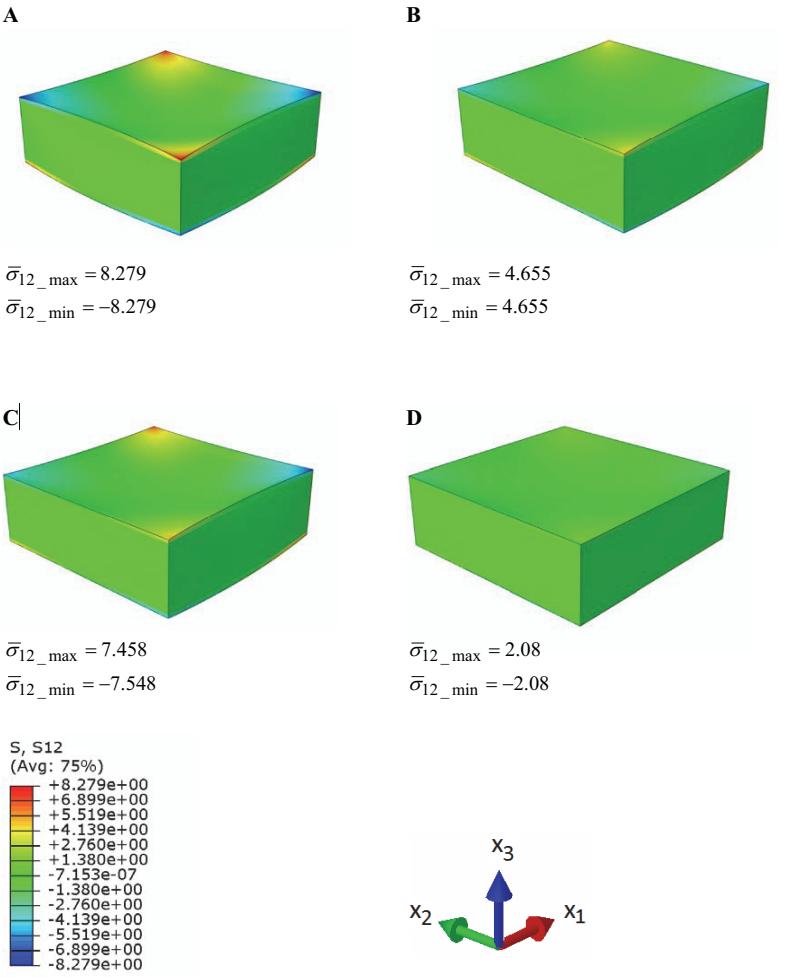


Figure 15. Distribution of in-plane shear stress $\bar{\sigma}_{12}$ for HC panel with (a) SSSS (b) CCSS (c) CSSS (d) CCCC boundary conditions.

displacements $\bar{u}_i = \dfrac{G_f u_i}{q_0 h}$ through the sandwich panel under the different boundary conditions.

The results are shown as either two- dimensional plots displaying stresses or displacement along a single line projected through the panel or as 3D images displaying the stress or displacement distribution across the panel as a whole.

Beginning with the through thickness variation of normalised out-of-plane normal stress $\bar{\sigma}_{33}$ (Fig. 12), it can be seen that under all boundary conditions and for both the FGMC and HC panels the plots are identical, showing that the type of core has very little effect on this stress component. It is believed that this is due to the effect of the mechanical properties of the face sheets which have a significant contribution on the through thickness behaviour of the sandwich panel.

The core has a very strong influence on the through-thickness variation of the in-plane normal stress $\bar{\sigma}_{11}$, shown in Figs 13 and 14 at the centre of the panel ($x_1 = 0{\cdot}5a$, $x_2 = 0{\cdot}5b$). The use of

https://doi.org/10.1017/S0001924000007648 Published online by Cambridge University Press

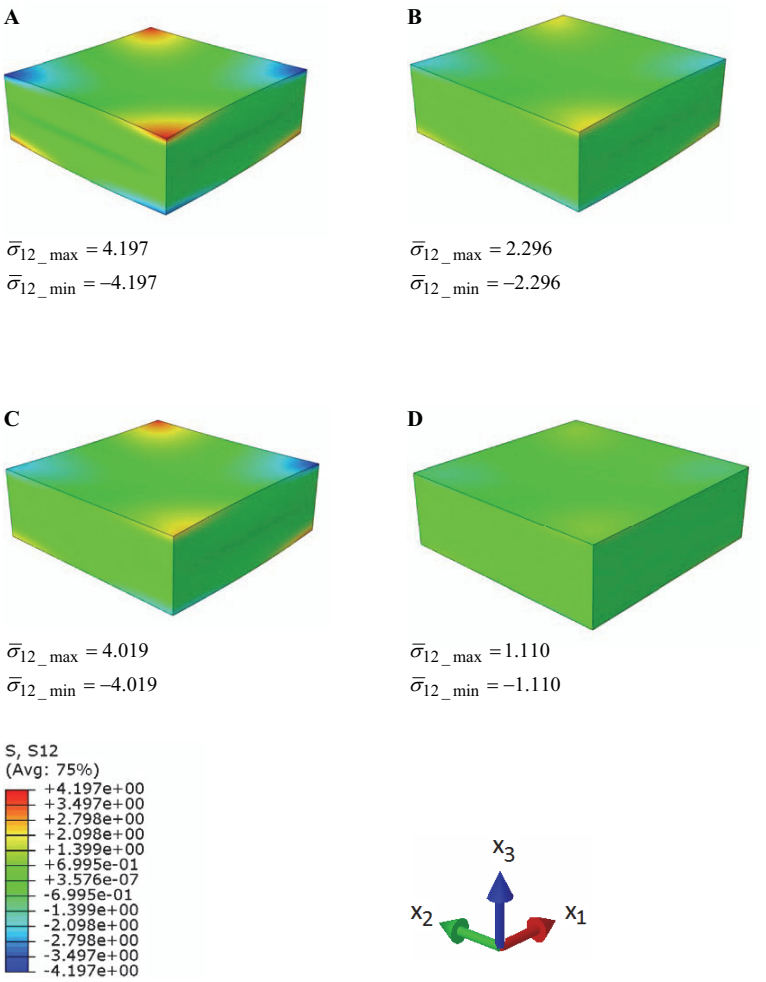


Figure 16. Distribution of in-plane shear stress $\bar{\sigma}_{12}$, for FGMC panel with (a) SSSS (b) CCSS (c) CSSS (d) CCCC boundary conditions.

functionally graded core not only eliminates the stress discontinuity across the face sheet/core interface, but also reduces the magnitude of stresses in the face sheets. This effect is observed under all of the studied boundary conditions, with the highest face sheet stresses occurring under CFFF and SSSS and the lowest under CFSF and FFSS conditions.

The distribution of in-plane shear stress $\bar{\sigma}_{12}$, is shown across the panel in Figs 15-20. Considering the individual boundary conditions in more detail, when comparing panels with all edges supported (i.e. SSSS, CCSS, CSSS and CCCC), it can be seen that the extremes of this stress component lie at the face sheet corners (Fig. 15 for HC panel, Fig. 16 for FGMC panel), reducing towards the centre. These stresses are higher in edges which are simply supported as since the rotation degree of freedom is not fixed (as it is in the clamped case), significantly more distortion of the original perpendicular element edges can occur. This stress is therefore at a maximum in panels where two simply supported edges meet since distortion can occur in both the $x_1$ and $x_2$ directions.

https://doi.org/10.1017/S0001924000007648 Published online by Cambridge University Press

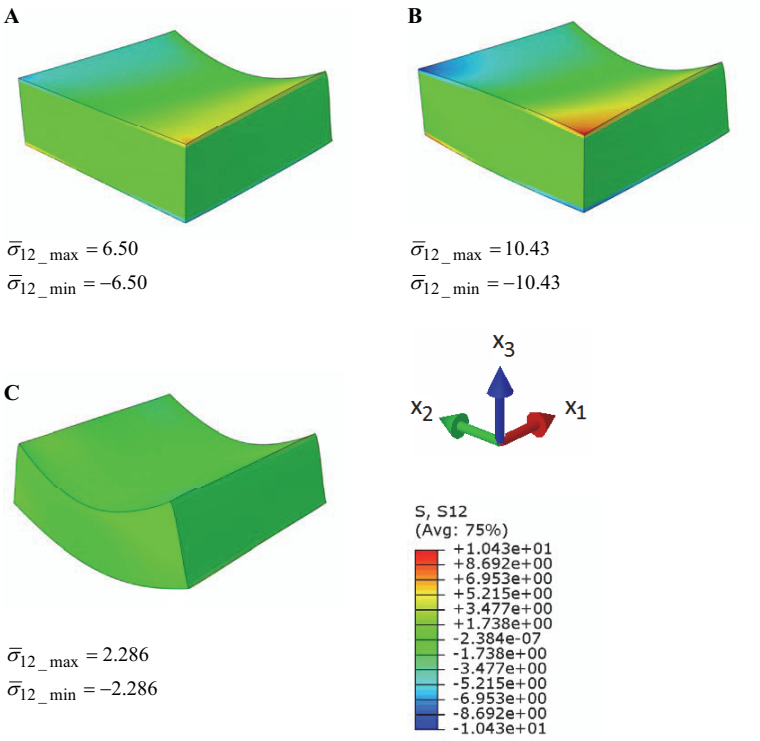


Figure 17. Distribution of in-plane shear stress $\bar{\sigma}_{12}$, for HC panel with (a) CFSS (b) SFSS (c) FFSS boundary conditions.

When considering panels with a free edge (Figs 17 and 19 for HC panel, Figs 18 and 20 for FGMC panel), since the boundary conditions state that the shear force is equal to zero on free edges, this stress component is zero along all free edges. The CFFF panels (Figs 19, 20(a)) show concentrations of shear stress where the free edge meets the clamped edge. This effect is mirrored in the CFSF panels (Figs 19, 20(b)) which also show high shear stresses along the simply supported edge (where maximum distortion is occurring).

There is once more a clear discontinuity across the face sheet-core interface for all of the panels with homogenous core, and the use of a FGM core once more eliminates this problem. It can also be seen that the introduction of the graded core decreases the magnitude of the transverse shear stresses by almost half under all boundary conditions considered.

Plots of through thickness variation of transverse shear stress $\bar{\sigma}_{13}$ at the centre of the panel ($x_1 = 0{\cdot}5a$, $x_2 = 0{\cdot}5b$) are shown in Figs 21 and 22. The highest transverse shear stresses are observed in a panel with three free edges (CFFF panel, Fig. 21), whereas in those cases when each pair of opposite edges has the same type of support (FFSS, SSSS, CCSS, CCCC) transverse shear stress $\bar{\sigma}_{13}$ vanishes (Figs 21, 22). The use of functionally graded core significantly reduces the magnitude of stresses in the face sheets and slightly increases it in the core.

The distribution of von Mises stresses across the panels is shown in Figs 23, 24 and 25 (for FGMC panel). Consideration of von Mises stress is of particular interest as it highlights which stress has the greatest effect in each of the cases considered. For panels with a clamped edge (Figs 23(b), (c), (d), 24(a) and 25(a), (b)) the normal stresses (due to bending) provide the greatest

https://doi.org/10.1017/S0001924000007648 Published online by Cambridge University Press

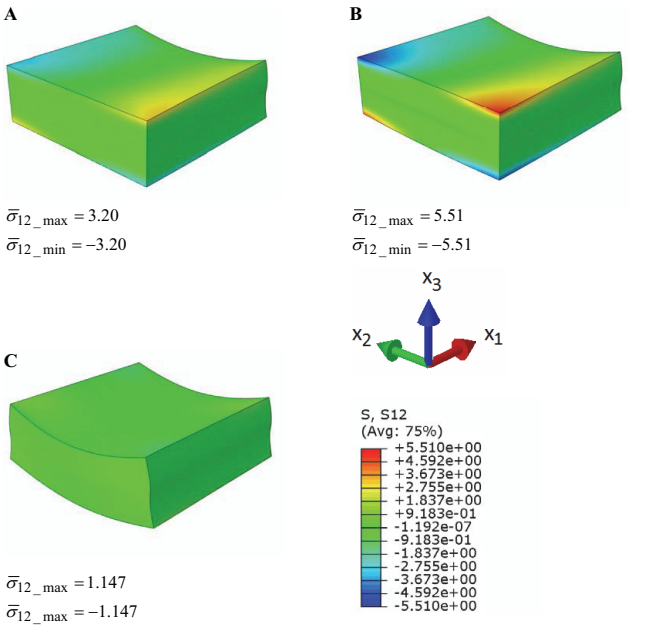


Figure 18. Distribution of in-plane shear stress $\bar{\sigma}_{12}$, for FGMC panel with (a) CFSS (b) SFSS (c) FFSS boundary conditions.

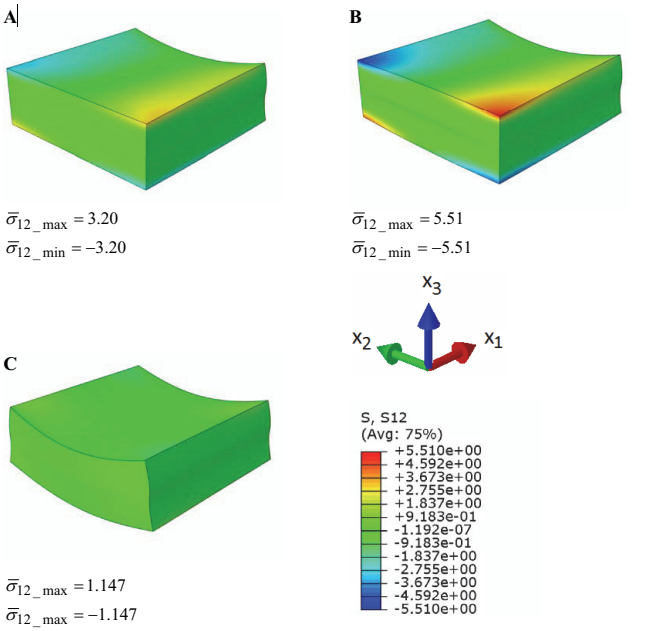


Figure 19. Distribution of in-plane shear stress $\bar{\sigma}_{12}$, for HC panel with (a) CFFF (b) CFSF boundary conditions.

https://doi.org/10.1017/S0001924000007648 Published online by Cambridge University Press

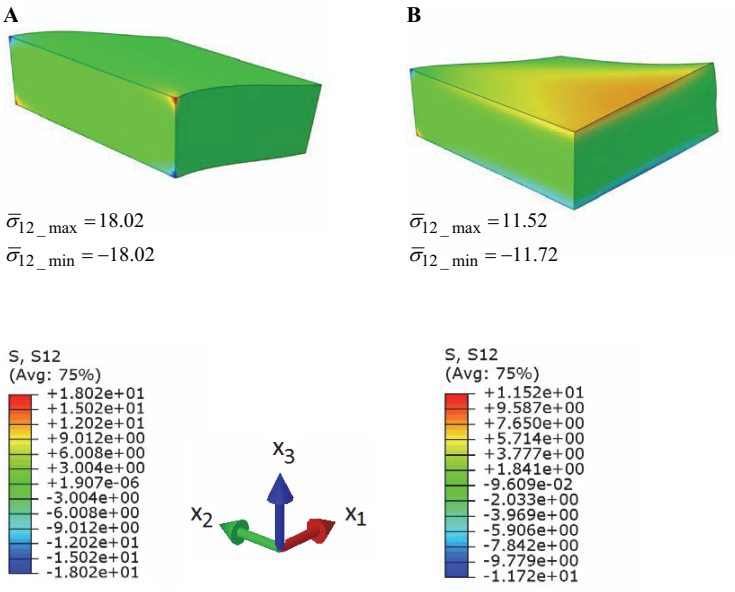


Figure 20. Distribution of in-plane shear stress $\bar{\sigma}_{12}$, for FGMC panel with (a) CFFF (b) CFSF boundary conditions.

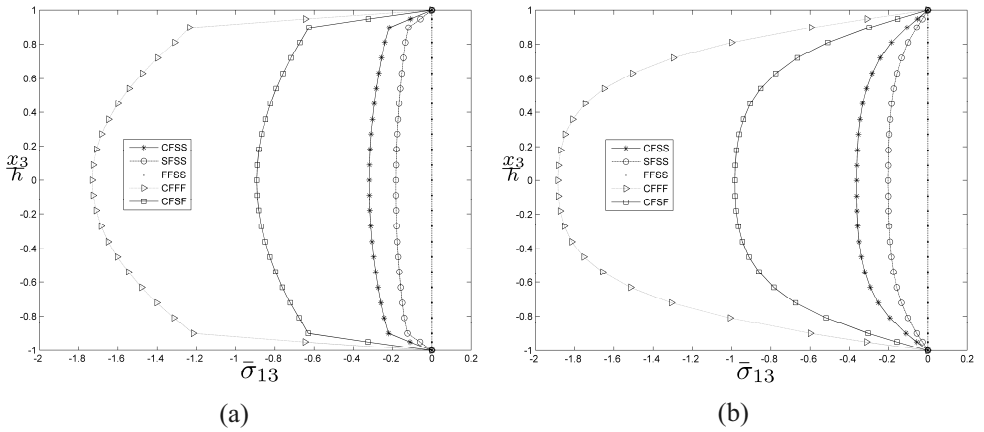


Figure 21. Through-thickness variation of the normalised transverse shear stress $\bar{\sigma}_{13}$ (0·5$a$, 0·5$b$, $x_3$) for a range of boundary conditions (CFSS, SFSS, FFSS, CFFF & CFSF) in (a) HC panel, (b) FGMC panel.

contribution to the overall stress distribution and this is highlighted by the stress concentration along these clamped edges. Conversely, along simply supported edges, the boundary conditions stipulate that the bending moment is equal to zero (and therefore normal stress are equal to zero) and as such the shear stress components provide far more of the overall von Mises stress. Therefore when considering the panels with no free edges (SSSS, CCSS, CSSS, CCCC) the maximum occurs where a clamped edge meets a simply supported edge and both normal and shear stresses make a significant contribution.

https://doi.org/10.1017/S0001924000007648 Published online by Cambridge University Press

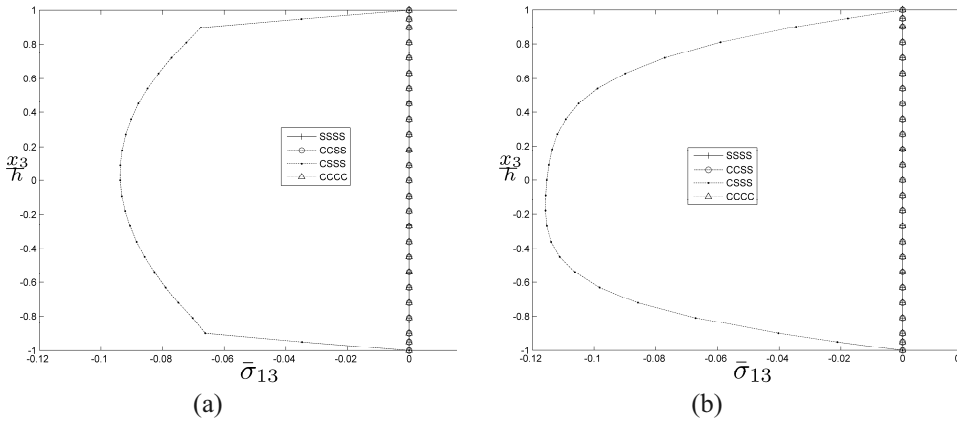


Figure 22. Through-thickness variation of the normalised transverse shear stress $\bar{\sigma}_{13}$ (0·5*a*, 0·5*b*, $x_3$) for a range of boundary conditions (SSSS, CCSS, CSSS & CCCC) in (b) HC panel, (b) FGMC panel.

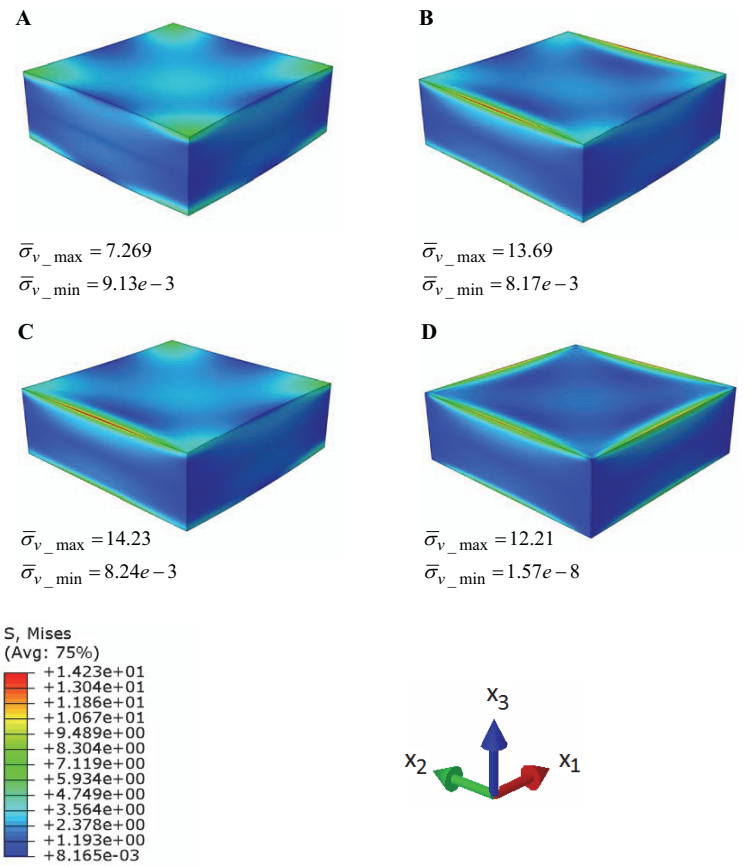


Figure 23. Distribution of son Mises stress $\bar{\sigma}_v$, for FGMC panel with (A) SSSS (B) CCSS (C) CSSS (D) CCCC boundary conditions.

https://doi.org/10.1017/S0001924000007648 Published online by Cambridge University Press

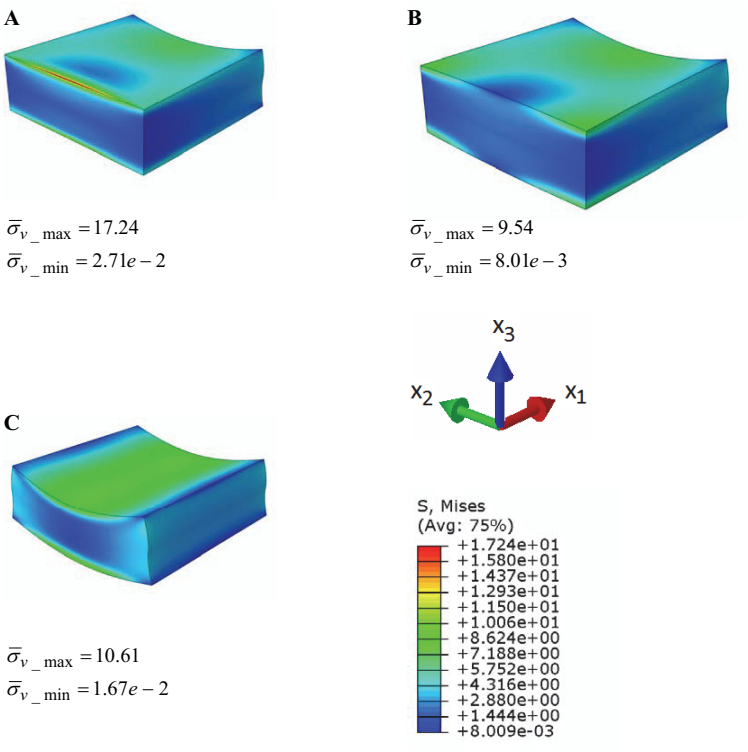


Figure 24. Distribution of von Mises stress $\bar{\sigma}_v$, for FGMC Panel with (a) CFSS (b) SFSS (c) FFSS.

In the cases involving a free edge, curvature of the panel at the upper and lower panel surfaces either in compression or tension once more becomes a factor and the bending stresses make a significant contribution. This can be seen particularly in the FFSS supported panel (Fig. 24(c)), which has low von Mises stresses near to the supports but higher stresses towards the centre due to the presence of the bending stresses $\bar{\sigma}_{11}$ and $\bar{\sigma}_2$. Plots for a panel containing HC core are not shown as the distributions in stress are similar to those for the FGM core. The differences are due to the discontinuities in in-plane normal and shear stresses which have already been highlighted in Figs 13, 14 and 15-20, respectively.

Considering the normalised transverse displacements $\bar{u}_3$ (Figs 26-29), the deformed shapes of the panel fall into two distinct categories. For panels with all edges supported (Fig. 26), the maximum deflection is in the centre of the panel ($0{\cdot}5a$, $0{\cdot}5b$); while for panels with one or more free edges, the maximum deflection lies under the free edge. For the CFSS and SFSS panels (Figs. 27(a), (b)), respectively) which have one free edge at $x_1 = a$, the maximum deflection lies at the mid point of this edge. Similarly, the FFSS panel (Fig. 27(c)), with free edges at $x_1 = 0,a$, the deflection is maximum along the centre of the panel (i.e. along the line $x_2 = b/2$). For the panel with CFFF boundary conditions (Fig. 28), the maximum deflection lies along the free edge at $x_1 = a$ and finally for the CFSF panel (Fig. 29), maximum deflection is at the point where the two free edges meet $x_1 = a$, $x_2 = b$. It can also be seen from this series of images, that as the panel is loaded, clamped edges remain perfectly straight whilst simply supported edges become curved. When comparing panels with homogenous and graded core, it was found that the increased

https://doi.org/10.1017/S0001924000007648 Published online by Cambridge University Press

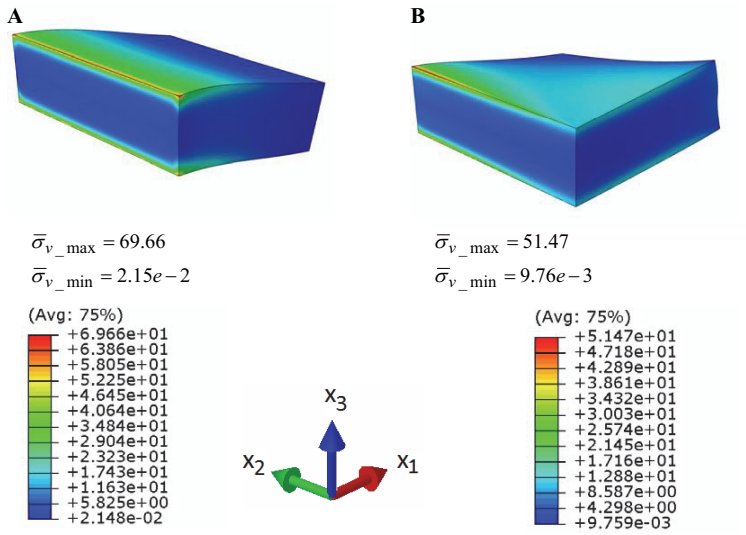


Figure 25. Distribution of von Mises stress $\bar{\sigma}_v$, for FGMC panel with (a) CFFF (b) CFSF boundary conditions.

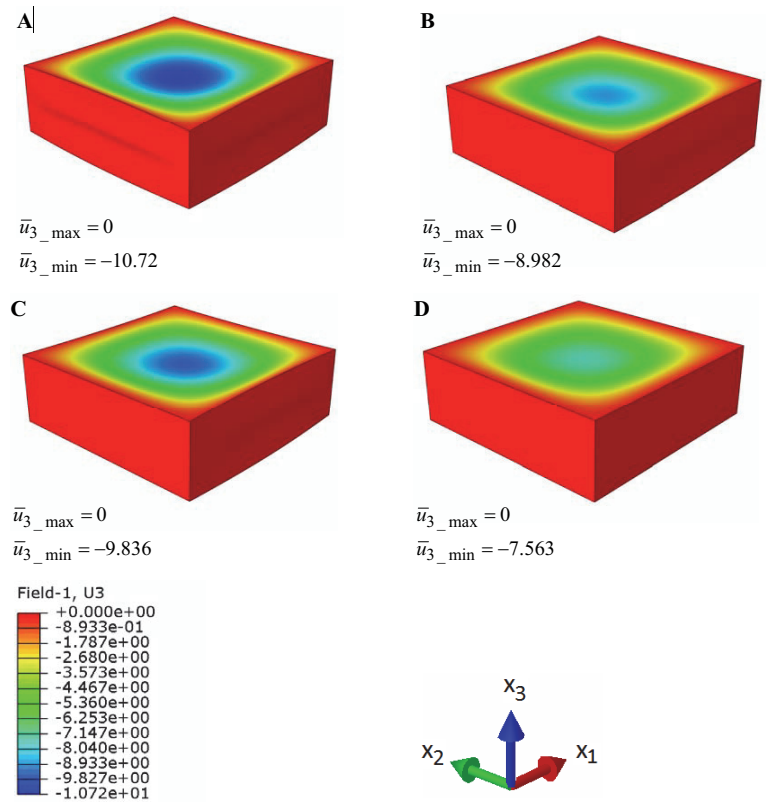


Figure 26. Distribution of transverse displacement $\bar{u}_3$, for FGMC panel with (a) SSSS (b) CCSS (c) CSSS (d) CCCC boundary conditions.

https://doi.org/10.1017/S0001924000007648 Published online by Cambridge University Press

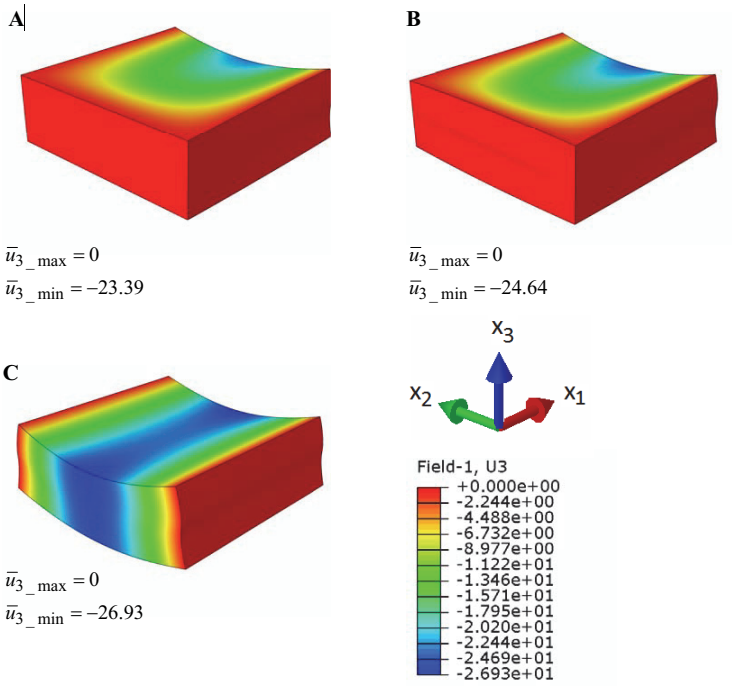


Figure 27. Distribution of transverse displacement $\bar{u}_3$, for FGMC panel with (a) CFSS (b) SFSS (c) FFSS boundary conditions.

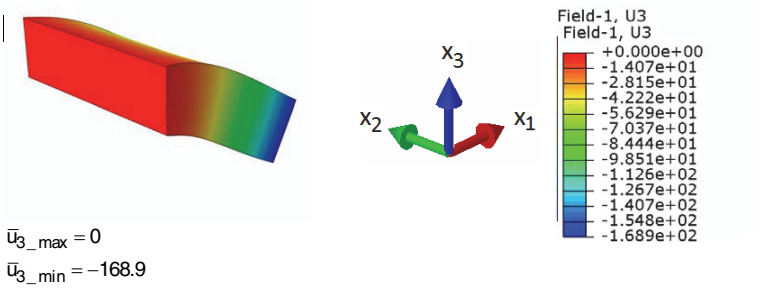


Figure 28. Distribution of transverse displacement $\bar{u}_3$, for FGMC panel with CFFF boundary conditions.

stiffness of the graded core reduces displacement throughout the panel (the panel with graded core would however come with a weight penalty over the panel with homogeneous core). This trend is seen under all boundary conditions. Looking at the individual boundary conditions in greater detail, reveals that panels with two or more free edges have the largest transverse displacements, followed by panels with one free edge, panels with multiple simply supported edges and finally the smallest displacements are seen for the panel multiple clamped edges, with the cantilever panel CFFF having maximum displacement over 20 times larger than the CCCC panel. (i.e. in order from largest to smallest to displacements — CFFF, CFSF, FFSS, SFSS, CFSS, SSSS, CSSS, CCSS, CCCC).

Finally, through-thickness variations of the in-plane displacements $\bar{u}_1$ (Fig. 30) shows that the panel behaves in a similar manner for all boundary conditions. The increased stiffness of the

https://doi.org/10.1017/S0001924000007648 Published online by Cambridge University Press

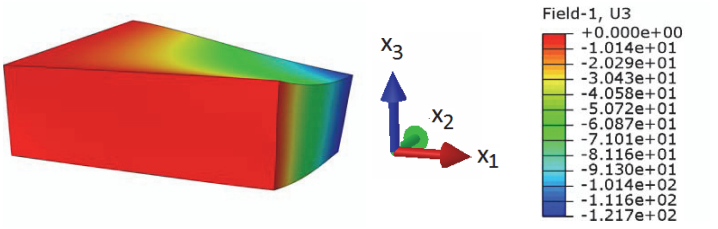


$\bar{u}_{3\_max} = 0$

$\bar{u}_{3\_min} = -121.7$

Figure 29. Distribution of transverse displacement $\bar{u}_3$, for FGMC panel with CFSF boundary conditions.

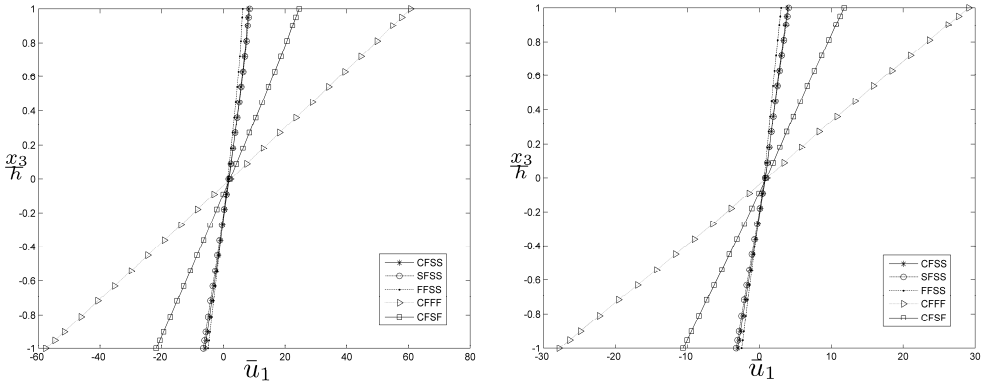


Figure 30. Through-thickness variation of the normalised in-plane displacement $\bar{u}_1(a, 0{\cdot}5b, x_3)$ for a range of boundary conditions (CFSS, SFSS, FFSS, CFFF & CFSF) in (a) HC panel, (b) FGMC panel.

graded core reduces displacement throughout the panel. The same pattern is observed as was seen for transverse displacements, with the panels with free edges showing the greatest displacements, followed by simply supported edges and then clamped edges minimising the displacement.

## 6.0 CONCLUSIONS

In the current paper, a sandwich panel containing a functionally graded core subjected to uniformly distributed under combinations of simply supported, clamped and free edges has been analysed using a 3D finite element method with user-implemented graded elements. Results were then compared with an equivalent panel containing homogenous core. It is seen that introduction of the functionally graded core removes the discontinuity in stresses at the interfaces and decreases both in- and out-of plane displacements for all of the boundary conditions considered. The panels with free edges were seen to have the greatest displacements, followed by panels with simply supported edges and those with clamped edges minimising the displacements.

https://doi.org/10.1017/S0001924000007648 Published online by Cambridge University Press

## ACKNOWLEDGEMENTS

Financial support of this research by the EPSRC DTA grant is gratefully acknowledged.

## REFERENCES

1. BESANT, T., DAVIES, G.A.O. and HITCHINGS, D. Finite element modelling of low velocity impact of composite panels, *Composites Part A: Applied Science and Manufacturing,* 2001, **32**, pp 1189-1196.
2. DAVIES, G.A.O., HITCHINGS, D., BESANT, T., CLARKE, A. and MORGAN, C. Compression after impact strength of composite sandwich panels, *Composite Structures*, 2004, **63**, (1), pp 1-9, 1999, **22**, (4): pp 477-512.
3. ANDERSON, T.A. A 3D elasticity solution for a sandwich composite with functionally graded core subjected to transverse loading by a rigid sphere, *Composite Structures*, 2003, **60**, (3), pp 265-74.
4. KASHTALYAN, M. and MENSHYKOVA, M. Three-dimensional elasticity solution for sandwich panels with a functionally graded core, *Composite Structures*, 2009, **87**, (1), pp 36-43.
5. WOODWARD, B. and KASHTALYAN, M. Bending response of sandwich panels with graded core: 3D elasticity analysis, *Mechanics of Advanced Materials and Structures,* 2010, **17**, (8), pp 586-594.
6. WOODWARD, B. and KASHTALYAN, M. 3D elasticity analysis of sandwich panels with graded core under distributed and concentrated loadings, *Int J Mechanical Sciences*, 2011, **53**, (10), pp 872-885.
7. APETRE, N.A., SANKAR, B.V. and AMBUR, D.R. Analytical modeling of sandwich beams with functionally graded core, *J Sandwich Structures and Materials*, 2008, **10**, (1), pp 53-74.
8. BIAN, Z.G., CHEN, W.Q., LIM, C.W. and ZHANG, N. Analytical solutions for single- and multi-span functionally graded plates in cylindrical bending, *Int J Solids and Structures*, 2005, **42**, (24-25), pp 6433-56.
9. ZHONG, Z. and YU, T. Analytical solution of a cantilever functionally graded beam, *Composites Science and Technology,* 2007, **67**, (3-4), pp 481-8.
10. XU, Y. and ZHOU, D. Three-dimensional elasticity solution of functionally graded rectangular plates with variable thickness, *Composite Structures*, 2009, **91**, (1), pp 56-65.
11. XU, Y., ZHOU, D. and CHEUNG, Y.K. Elasticity solution of clamped-simply supported beams with variable thickness, *Applied Mathematics and Mechanics (English Edition)*, 2008, **29**, (3), pp 279-90.
12. HUANG, Z.Y., LÜ, C.F. and CHEN, W.Q. Benchmark solutions for functionally graded thick plates resting on Winkler-Pasternak elastic foundations, *Composite Structures*, 2008, **85**, (2), pp 95-104.
13. SBURLATI, R. and BARDELLA, L. Three-dimensional elastic solutions for functionally graded circular plates, *European J Mechanics — A/Solids*, 2011, **30**, (3), pp 219-35.
14. KIM, J. and PAULINO, G.H. Isoparametric graded finite elements for nonhomogeneous isotropic and orthotropic materials, *Transactions ASME J Applied Mechanics*, 2002, **69**, (4), pp 502-14.
15. BUTTLAR, W.G., PAULINO, G.H. and SONG, S.H. Application of graded finite elements for asphalt pavements, *J Engineering Mechanics*, 2006, **132**, (3), pp 240-8.
16. SANTARE, M.H. and LAMBROS, J. Use of graded finite elements to model the behaviour of nonhomogeneous materials, *J Applied Mechanics*, 2000, **67**, pp 819-22.
17. LI, C. and ZOU, Z. Multiple isoparametric finite element method for nonhomogeneous media, *Mechanics Research Communication*s, 2000, **27**, (2), pp 137-42.
18. ASTLEY, R.J. *Finite Elements in Solids and Structures, an Introduction*, 1992, Chapman and Hall, London.
19. ZIENKIEWICZ, O.C. and TAYLOR, R.L. *The Finite Element Method*, 1990, McGraw-Hill, London.
20. Dassault Systèmes. ABAQUS version 6.8 Documentation, 2008.
21. WOODWARD, B. and KASHTALYAN, M. Performance of functionally graded plates under localised transverse loadings, *Composite Structures*, 2012, **94**, (7), pp 2254-2262.
22. KASHTALYAN, M. Three-dimensional elasticity solution for bending of functionally graded rectangular plates, *European J Mechanics A/Solids*, 2004, **23**, (5), pp 853-864.
23. REDDY, J.N. *Theory and Analysis of Elastic Plates and Shells,* Second edition, 2007, CRC Press, Boca Raton.

# APPENDIX

Using the displacement function method, 3D representation of displacement and stress fields in a simply-supported sandwich panel with functionally graded core has been obtained[6] as:

$$u_1^{(k)} = \sum_{m=1}^{\infty}\sum_{n=1}^{\infty}\sum_{j=1}^{6} A_{j,mn}^{(k)} U_{1,jmn}^{(k)}(x_3)\,\mathrm{Cos}\frac{\pi m x_1}{a}\,\mathrm{Sin}\frac{\pi n x_2}{b} \quad \ldots (A1a)$$

$$u_2^{(k)} = \sum_{m=1}^{\infty}\sum_{n=1}^{\infty}\sum_{j=1}^{6} A_{j,mn}^{(k)} U_{2,jmn}^{(k)}(x_3)\,\mathrm{Sin}\frac{\pi m x_1}{a}\,\mathrm{Cos}\frac{\pi n x_2}{b} \quad \ldots (A1b)$$

$$u_3^{(k)} = \sum_{m=1}^{\infty}\sum_{n=1}^{\infty}\sum_{j=1}^{6} A_{j,mn}^{(k)} U_{3,jmn}^{(k)}(x_3)\,\mathrm{Sin}\frac{\pi m x_1}{a}\,\mathrm{Sin}\frac{\pi n x_2}{b} \quad \ldots (A1c)$$

$$\sigma_{33}^{(k)} = \sum_{m=1}^{\infty}\sum_{n=1}^{\infty}\sum_{j=1}^{6} A_{j,mn}^{(k)} P_{33,jmn}^{(k)}(x_3)\,\mathrm{Sin}\frac{\pi m x_1}{a}\,\mathrm{Sin}\frac{\pi n x_2}{b} \quad \ldots (A2a)$$

$$\sigma_{13}^{(k)} = \sum_{m=1}^{\infty}\sum_{n=1}^{\infty}\sum_{j=1}^{6} A_{j,mn}^{(k)} P_{13,jmn}^{(k)}(x_3)\,\mathrm{Cos}\frac{\pi m x_1}{a}\,\mathrm{Sin}\frac{\pi n x_2}{b} \quad \ldots (A2b)$$

$$\sigma_{23}^{(k)} = \sum_{m=1}^{\infty}\sum_{n=1}^{\infty}\sum_{j=1}^{6} A_{j,mn}^{(k)} P_{23,jmn}^{(k)}(x_3)\,\mathrm{Sin}\frac{\pi m x_1}{a}\,\mathrm{Cos}\frac{\pi n x_2}{b} \quad \ldots (A2c)$$

$$\sigma_{11}^{(k)} = \sum_{m=1}^{\infty}\sum_{n=1}^{\infty}\sum_{j=1}^{6} A_{j,mn}^{(k)} P_{11,jmn}^{(k)}(x_3)\,\mathrm{Sin}\frac{\pi m x_1}{a}\,\mathrm{Sin}\frac{\pi n x_2}{b} \quad \ldots (A2d)$$

$$\sigma_{22}^{(k)} = \sum_{m=1}^{\infty}\sum_{n=1}^{\infty}\sum_{j=1}^{6} A_{j,mn}^{(k)} P_{22,jmn}^{(k)}(x_3)\,\mathrm{Sin}\frac{\pi m x_1}{a}\,\mathrm{Sin}\frac{\pi n x_2}{b} \quad \ldots (A2e)$$

$$\sigma_{12}^{(k)} = \sum_{m=1}^{\infty}\sum_{n=1}^{\infty}\sum_{j=1}^{6} A_{j,mn}^{(k)} P_{12,jmn}^{(k)}(x_3)\,\mathrm{Cos}\frac{\pi m x_1}{a}\,\mathrm{Cos}\frac{\pi n x_2}{b} \quad \ldots A2f)$$

For any pair of $m$ and $n$, $A_{j,mn}^{(k)}$ are sets of 24 arbitrary constants to be determined from the boundary conditions on the top and bottom surfaces of the panel as well continuity conditions, Equation (3); $U_{1,jmn}^{(k)}$, $U_{2,jmn}^{(k)}$, $U_{3,jmn}^{(k)}$, $P_{33,jmn}^{(k)}$, $P_{13,jmn}^{(k)}$, $P_{23,jmn}^{(k)}$, $P_{11,jmn}^{(k)}$, $P_{22,jmn}^{(k)}$ and $P_{12,jmn}^{(k)}$ are

Functions $U_{i,jmn}^{(k)}$ and $P_{rt,jmn}^{(k)}$ involved in Equations (1a-c) and Equations (2a-f)

$$U_{1,jmn}^{(k)}(\bar{x}_3) = -\frac{q_{mn}h}{2g^{(k)}}\frac{\pi m h}{a}\exp[-\gamma^{(k)}(\bar{x}_3-1)]\left[-\nu^{(k)}\alpha^2 h^2 f_j^{(k)}(\bar{x}_3) + (\nu^{(k)}-1)\frac{\mathrm{d}^2}{\mathrm{d}\bar{x}_3^2} f_j^{(k)}(\bar{x}_3)\right]$$

$$U_{2,jmn}^{(k)}(\bar{x}_3) = -\frac{q_{mn}h}{2g^{(k)}}\frac{\pi n h}{b}\exp[-\gamma^{(k)}(\bar{x}_3-1)]\left[-\nu^{(k)}\alpha^2 h^2 f_j^{(k)}(\bar{x}_3) + (\nu^{(k)}-1)\frac{\mathrm{d}^2}{\mathrm{d}\bar{x}_3^2} f_j^{(k)}(\bar{x}_3)\right]$$

$$U_{3,jmn}^{(k)}(\bar{x}_3) = -\frac{q_{mn}h}{2g^{(k)}}\frac{\pi m h}{a}\exp[-\gamma^{(k)}(\bar{x}_3-1)]\left[(\nu^{(k)}-1)\left(-\gamma^{(k)}\frac{\mathrm{d}^2}{\mathrm{d}\bar{x}_3^2} f_j^{(k)}(\bar{x}_3) + \frac{\mathrm{d}^3}{\mathrm{d}\bar{x}_3^2} f_j^{(k)}(\bar{x}_3)\right)\right.$$
$$\left. -\alpha^2 h^2\left((\nu^{(k)}-2)\frac{\mathrm{d}}{\mathrm{d}\bar{x}_3} f_j^{(k)}(\bar{x}_3) - \nu^{(k)}\gamma^{(k)} f_j^{(k)}(\bar{x}_3)\right)\right], \quad j=1,\ldots,4;$$

$$U_{1,jmn}^{(k)}(\bar{x}_3) = -\frac{q_{mn}h}{g^{(k)}}\frac{\pi n h}{b} f_j^{(k)}(\bar{x}_3)$$

https://doi.org/10.1017/S0001924000007648 Published online by Cambridge University Press

$$U^{(k)}_{2,jmn}(\bar{x}_3) = \frac{q_{mn}h}{g^{(k)}}\frac{\pi mh}{a} f^{(k)}_j(\bar{x}_3)$$

$$U^{(k)}_{3,jmn}(\bar{x}_3) = 0, \quad j = 5,6;$$

$$P^{(k)}_{33,jmn}(\bar{x}_3) = q_{mn}\alpha^4 h^4 f^{(k)}_j(\bar{x}_3)$$

$$P^{(k)}_{13,jmn}(\bar{x}_3) = q_{mn}\alpha^2 h^2 \left(\frac{\pi mh}{a}\right)\frac{\mathrm{d}}{\mathrm{d}\bar{x}_3} f^{(k)}_j(\bar{x}_3)$$

$$P^{(k)}_{23,jmn}(\bar{x}_3) = q_{mn}\alpha^2 h^2 \left(\frac{\pi nh}{b}\right)\frac{\mathrm{d}}{\mathrm{d}\bar{x}_3} f^{(k)}_j(\bar{x}_3)$$

$$P^{(k)}_{11,jmn}(\bar{x}_3) = q_{mn}\left[\nu^{(k)}\alpha^2 h^2\left(\frac{\pi nh}{b}\right)^2 f^{(k)}_j(\bar{x}_3) - \nu^{(k)}\left(\frac{\pi nh}{b}\right)^2 \frac{\mathrm{d}^2}{\mathrm{d}\bar{x}_3^2} f^{(k)}_j(\bar{x}_3) - \left(\frac{\pi mh}{a}\right)^2 \frac{\mathrm{d}^2}{\mathrm{d}\bar{x}_3^2} f^{(k)}_j(\bar{x}_3)\right]$$

$$P^{(k)}_{22,j}(\bar{x}_3) = q_{mn}\left[\nu^{(k)}\alpha^2 h^2\left(\frac{\pi mh}{a}\right)^2 f^{(k)}_j(\bar{x}_3) - \nu^{(k)}\left(\frac{\pi mh}{a}\right)^2 \frac{\mathrm{d}^2}{\mathrm{d}\bar{x}_3^2} f^{(k)}_j(\bar{x}_3) - \left(\frac{\pi nh}{b}\right)^2 \frac{\mathrm{d}^2}{\mathrm{d}\bar{x}_3^2} f^{(k)}_j(\bar{x}_3)\right]$$

$$P^{(k)}_{12,jmn}(\bar{x}_3) = q_{mn}\left(\frac{\pi mh}{a}\right)\left(\frac{\pi nh}{b}\right)\left[\nu^{(k)}\alpha^2 h^2 f^{(k)}_j(\bar{x}_3) + (1-\nu^{(k)})\frac{\mathrm{d}^2}{\mathrm{d}\bar{x}_3^2} f^{(k)}_j(\bar{x}_3)\right], \; j = 1,\ldots,4$$

$$P^{(k)}_{33,jmn}(\bar{x}_3) = 0$$

$$P^{(k)}_{13,jmn}(\bar{x}_3) = -q_{mn}\left(\frac{\pi nh}{b}\right)\exp\left[\gamma^{(k)}\left(\frac{x_3}{h} - 1\right)\right]\frac{\mathrm{d}}{\mathrm{d}\bar{x}_3} f^{(k)}_j(\bar{x}_3)$$

$$P^{(k)}_{23,j}(\bar{x}_3) = q_{mn}\left(\frac{\pi mh}{a}\right)\exp[\gamma^{(k)}(\bar{x}_3 - 1)]\frac{\mathrm{d}}{\mathrm{d}\bar{x}_3} f^{(k)}_j(\bar{x}_3)$$

$$P^{(k)}_{11,jmn}(\bar{x}_3) = 2q_{mn}\left(\frac{\pi nh}{b}\right)\left(\frac{\pi mh}{a}\right)\exp[\gamma^{(k)}(\bar{x}_3 - 1)] f^{(k)}_j(\bar{x}_3)$$

$$P^{(k)}_{22,jmn}(\bar{x}_3) = -2q_{mn}\left(\frac{\pi nh}{b}\right)\left(\frac{\pi mh}{a}\right)\exp[\gamma^{(k)}(\bar{x}_3 - 1)] f^{(k)}_j(\bar{x}_3)$$

$$P^{(k)}_{12,jmn}(\bar{x}_3) = q_{mn}\left[\left(\frac{\pi mh}{a}\right)^2 - \left(\frac{\pi nh}{b}\right)^2\right]\exp[\gamma^{(k)}(\bar{x}_3 - 1)] f^{(k)}_j(\bar{x}_3), \; j = 5,6$$

In the expressions above, $\bar{x}_3 = x_3/h$, and functions $f^{(k)}_j(\bar{x}_3)$ $(j = 1, \ldots, 6)$ are

$$f^{(k)}_1(\bar{x}_3) = \exp\left(\frac{\gamma^{(k)}\bar{x}_3}{2}\right)\mathrm{Cosh}\lambda^{(k)}\bar{x}_3\mathrm{Cos}\mu^{(k)}\bar{x}_3$$

$$f^{(k)}_2(\bar{x}_3) = \exp\left(\frac{\gamma^{(k)}\bar{x}_3}{2}\right)\mathrm{Sinh}\lambda^{(k)}\bar{x}_3\mathrm{Cos}\mu^{(k)}\bar{x}_3$$

https://doi.org/10.1017/S0001924000007648 Published online by Cambridge University Press

$$f_3^{(k)}(\overline{x}_3) = \exp\left(\frac{\gamma^{(k)}\overline{x}_3}{2}\right)\mathrm{Cosh}\lambda^{(k)}\overline{x}_3\mathrm{Sin}\mu^{(k)}\overline{x}_3$$

$$f_4^{(k)}(\overline{x}_3) = \exp\left(\frac{\gamma^{(k)}\overline{x}_3}{2}\right)\mathrm{Sinh}\lambda^{(k)}\overline{x}_3\mathrm{Sin}\mu^{(k)}\overline{x}_3$$

$$f_5^{(k)}(\overline{x}_3) = \exp\left(-\frac{\gamma^{(k)}\overline{x}_3}{2}\right)\mathrm{Cosh}\beta^{(k)}\overline{x}_3$$

$$f_6^{(k)}(\overline{x}_3) = \exp\left(-\frac{\gamma^{(k)}\overline{x}_3}{2}\right)\mathrm{Sinh}\beta^{(k)}\overline{x}_3$$

where

$$\begin{pmatrix}\lambda^{(k)}\\ \mu^{(k)}\end{pmatrix} = \sqrt{\frac{1}{2}\left(\pm\beta^{(k)2} + \sqrt{\beta^{(k)4} + \gamma^{(k)2}\alpha^2 h^2\frac{\nu^{(k)}}{1-\nu^{(k)}}}\right)}, \quad \alpha = \pi\sqrt{\left(\frac{m}{a}\right)^2 + \left(\frac{n}{b}\right)^2}$$

$$\beta^{(k)} = \sqrt{\frac{\gamma^{(k)2}}{4} + \alpha^2 h^2} \text{ and } g^{(k)} = G^{(k)}(h)$$

https://doi.org/10.1017/S0001924000007648 Published online by Cambridge University Press